

## Cation exchange capacity and water content of opal in sedimentary basins: Example from the Monterey Formation, California

ARKADIUSZ DERKOWSKI<sup>\*1</sup>, JAN ŚRODOŃ<sup>1</sup> AND DOUGLAS K. MCCARTY<sup>2</sup>

<sup>1</sup>Institute of Geological Sciences, Polish Academy of Sciences, Senacka 1, Kraków, 31-002 Poland

<sup>2</sup>Chevron ETC, 3901 Briarpark Drive, Houston, Texas 77042, U.S.A.

### ABSTRACT

Surface characteristics of sedimentary opal-A and -CT were investigated for a large collection of samples from the Monterey Formation, California, based on the bulk rock mineral and chemical analysis, cation exchange capacity (CEC), and water content. Two approaches were used: (1) modeling bulk CEC and adsorbed water content for the entire data set using the contents of opal and clay minerals measured by XRD, and (2) correcting the chemical composition and CEC of the most pure opal samples for the mineral impurities quantified by XRD.

Modeling indicates that the bulk rock data can be best explained by mixing an illite-smectite (CEC = 59 meq/100 g, 7–8% H<sub>2</sub>O), consistent with the XRD characteristics of the clay fraction, with opal-A (8 meq/100 g, 3.4% H<sub>2</sub>O), and opal-CT (13 meq/100 g, 3.7% H<sub>2</sub>O).

Correcting the chemical composition of the most pure opal samples leaves a large excess of cations (Al, Fe, Na, K, Ca, and Mg). Iron is suspect to form traces of separate (oxy-)hydroxide phases, not detected by XRD, while Al for Si substitution in the opal structure produced local negative charge, which was compensated by Na, K, Ca, and Mg exchange cations. A perfect balance of positive and negative charges is observed if the clay admixture in pure opals has the composition of montmorillonite. The concentration of heterogeneous impurities in silica network in opal leads to smectite formation on or within the diatom frustules. These dispersed smectite particles, perhaps monolayers, can be missed during the bulk rock mineral quantification.

The recalculated CEC of the opal, assuming the occurrence of dispersed smectite particles, varies from 3 to 11 meq/100 g, which is slightly less than that evaluated by modeling all the rock samples in the set, and corresponds to ~10–50% of the total opal charge quantified by the degree of Al for Si substitution. The remaining charge of the opal structure represents non-exchangeable cations. As opposed to smectite, opal CEC may depend on the size of cation used for the CEC measurement.

For opals in the Monterey Formation the content of water removable at 200 °C can be modeled as a sum of a constant value and a variable value dependent on CEC; the latter component is similar to the H<sub>2</sub>O-CEC relationship that is typical for smectite. The combined system of a constant H<sub>2</sub>O + variable H<sub>2</sub>O in opal can potentially be applied for mineral modeling programs in wireline log formation evaluation in diatomaceous hydrocarbon reservoirs.

**Keywords:** Adsorbed water, cation exchange capacity, illite-smectite, Monterey Formation, opal, smectite

### INTRODUCTION

Cation exchange capacity (CEC) is among the most important physicochemical properties of sedimentary rocks. In the oil and gas industry, the CEC value reflects the quantity of hydrated cations, allows calculation of the mineral surface-bound water, and is used for various corrections and calibrations in wireline log analysis where it is employed in calculating effective porosity and permeability in hydrocarbon reservoirs (Clavier et al. 1984; Fertl and Chilingar 1988; Brown and Ransom 1996; Matteson et al. 2000). CEC is also important to hydrocarbon production, where it relates to formation damage potential, affects drilling and completion strategies, and is needed to design effective

reservoir stimulation techniques.

One of the most common paradigms in measuring and modeling the sedimentary rock surface properties is the assumption that the bulk rock CEC and the total specific surface area (TSSA) are interrelated and control the quantity of adsorbed water via the content of hydrated cations, while CEC and TSSA of zeolite-free rocks are controlled almost exclusively by the quantity and type of clay minerals in a rock (Fertl and Chilingar 1988; Kaufhold 2006; Środoń and McCarty 2008; Środoń 2009; Środoń et al. 2009; Kaufhold et al. 2010). Therefore, the total adsorbed water in a sedimentary rock is essentially that of the clay-bound water (CBW). Clay minerals, including smectite, mixed-layered illite-smectite (I-S), and other less-common expandable mixed-layered clays (i.e., chlorite-smectite and kaolinite-smectite), contribute to the bulk CEC and TSSA, proportionally to their content in the

\* E-mail: [ndderkow@cyf-kr.edu.pl](mailto:ndderkow@cyf-kr.edu.pl)

rock, their expandability (%S; percentage of smectitic surfaces and interlayers), and the surface charge density ( $Q_s$ ). Discrete illite has a CEC of about 15–20 meq/100 g (Środoń et al. 2009) and is a minor contributor to the bulk CEC, while other micas and non-expandable clays, like chlorite and kaolinite, have negligible impact on the bulk CEC. In common diagenetic environments, such as sand-shale reservoirs, the typical range of CEC values of the smectitic end-member of I-S is limited because of the narrow range of its layer charge density:  $Q_s = 0.42 \pm 0.03$  (Środoń 2009), which translates to the average CEC of ~110 meq/100 g. Due to the narrow range of I-S surface charge densities and the fact that common pure smectite also has an average CEC value of 100 meq/100 g (Środoń and McCarty 2008), the measured bulk CEC roughly represents the sum of smectitic surfaces in the sample. The CBW content is then directly calculated from the bulk, measured CEC (Clavier et al. 1984). In common sedimentary rocks, %S and weight percent of I-S and illite are the main factors determining bulk rock CEC and CBW. Rare sediments rich in zeolites do not follow this rule (Derkowski et al. 2006).

Opal derived from biogenic silica form a significant portion of mineral matrix in pelagic sediments, deposited in the upwelling zones. Because of the porous construction of the original diatom frustules, these deposits can have very high porosity and thus become exceptionally good hydrocarbon reservoirs (Montgomery and Morea 2001; Cortese et al. 2004; Shukla and Mohan 2012). After deposition, the silica occurs as opal-A (amorphous) and, with increasing diagenesis, it transforms into opal of a mixed cristoballite-tridymite layer structure (opal-CT) with progressively decreasing tridymite content, then into opal-C, which finally recrystallizes into quartz (Williams and Crerar 1985; Guthrie et al. 1995; Elzea and Rice 1996).

Natural opal as well as its synthetic analog were found to possess various significant surface properties. Opal surface Si-OH groups provide a pH-dependent proton surface charge that varies among natural opal structures (Rodrigues et al. 2001; Khraisheh et al. 2005; Loucaides et al. 2010; Boboń et al. 2011; Ma et al. 2012). Aluminum dissolved in sea water complexes at the silica surface and can be incorporated into the silica structure (Gehlen et al. 2002; Koning et al. 2007; Houston et al. 2008). Substitution of Al and Fe for Si in the silica-silicate network is believed to produce local charge deficiency, which is compensated by the exchangeable Na, Ca, K, Ba, and Mg cations (Beck et al. 2002; Gehlen et al. 2002; Gaillou et al. 2008; Rondeau et al. 2012), as in phyllosilicates. The opal surface charge strongly increases opal reactivity potential, raising a question of opal behavior during CEC measurements. For example, Robertson and Twedily (1953) measured a very high CEC in pure diatoms, up to 54 meq/100 g using exchange with ammonia, but only a fraction of this value was measured using methylene blue. Moreover, a reaction of diatom frustules with saline water can result in significant incorporation of a mixture of cations in the opal structure, which in turn can produce authigenic smectite particles on or within diatom frustules (Van Bennekom and van der Gaast 1976; Badaut and Risacher 1983; Michalopoulos et al. 2000; Gehlen et al. 2002).

Natural opals are known to contain large quantities of water, both in H<sub>2</sub>O and OH forms, up to 15 wt%, in both opal-A and opal-CT structures (Jones and Renaut 2004; Boboń et al. 2011).

The thermal release of the water species (dehydration and dehydroxylation) occurs at different ranges of temperature with overlapping boundaries between them, but the majority is usually released below 500 °C (Graetsch et al. 1985; Mendioroz et al. 1989; Jones and Renaut 2004). Webb and Finlayson (1987) linked different quantities of molecular H<sub>2</sub>O and OH groups to the Mg and Al substitutions in Si framework.

Regardless the actual origin and type of the opal surface charge, opal surface properties and water content are expected to affect the petrophysical properties of the rock matrix in diatomaceous sedimentary basins, and in particular the bulk rock CEC. The CEC/CBW ratio could then be different than that known for clay minerals. The aim of this paper is to evaluate the large-scale potential contribution of opals to the reservoir CEC and the adsorbed water content, using a broad data set collected from the classic siliceous shale of the Monterey Formation in California.

## SAMPLES AND METHODS

Two types of samples were used in this study:

(1) Mineral standards. The standards represent several opal-A samples, a mixed-layer opal-CT, opal-C, and tridymite obtained from various sources, purified by chemical treatment and centrifugation. Structure and purity of the standards were checked by X-ray diffraction (XRD). Volcanic glass (obsidian) was used as a natural amorphous silica-rich reference to compare with the opal analysis.

(2) Natural samples from an opal-rich hydrocarbon reservoir. Over 300 core samples were collected from numerous wells drilled by Chevron's San Joaquin Valley Business Unit in the Antelope shale of the Monterey Formation, San Joaquin Basin, California, U.S.A. (Montgomery and Morea 2001). The samples represent an entire range of depths corresponding to the zones dominated by opal-A (~1000–1500 ft in the study area) and the zones rich in opal-CT containing usually >70% of cristobalite layers (~1300–1900 ft) (Elzea and Rice 1996; Chaika and Williams 2001). The actual well names, locations, and sampling depths cannot be revealed due to industrial confidentiality.

Portions of mineral standards equilibrated at  $50 \pm 3\%$  relative humidity (RH) were analyzed for water loss at 110 and 200 °C (labeled H<sub>2</sub>O110 and H<sub>2</sub>O200, respectively) when held for 15 min at a given temperature, using the Mettler-Toledo HR83 moisture analyzer. According to Środoń and McCarty (2008) and Środoń et al. (2009), drying at 200 °C is required to determine complete water loss from natural samples. The mineral standards were also analyzed for the continuous mass loss during heating by thermogravimetry (TG) using the TA 2050 analyzer connected to a mass spectrometer (MS) for evolved gas analysis. In the TG analysis ~25 mg of a sample was heated from room temperature to 1000 °C, with a rate of 5 °C/min, under N<sub>2</sub> gas flow of 25 mL/min.

All natural samples and mineral standards were analyzed for CEC using a broadly applied, accurate, and fast spectroscopic method of CEC determination via exchange with colorizing complex cations of high selectivity (Dohrmann 2006 and references therein). In this study CEC was determined using VIS spectrometry and hexaminecobalt(III) chloride solution at buffered pH ~7, following the method of Orsini and Remy (1976) and Bardón et al. (1993). A pre-dried sample (0.5–1 g) was mixed with 25 mL of the hexaminecobalt(III) stock solution at one of the absolute concentrations of 14.95, 7.48, 3.74, and 1.5 mmol, shaken and treated with ultrasounds for 2 min, then centrifuged for 10 min at ~4000 g. The absorbance of the supernatant solution, analyzed at a wavelength of 470 nm linearly depends on the amount of  $[\text{Co}(\text{NH}_3)_6]^{3+}$  cation, adsorbed by the tested sample.

Quantitative mineral analysis of bulk natural samples was performed using XRD analysis on Thermo-X'TRA diffractometer and the Quanta software (Chevron ETC proprietary), which uses the mineral intensity factor method in conjunction with a collection of pure standards (Środoń et al. 2001; Omotoso et al. 2006). The sample preparation procedure applied for the samples was described by Środoń et al. (2001). The Quanta XRD standards contain a selection of disordered and partially ordered structures of clay minerals and opal of various types and the approach used has been proven successful in opal-rich and clay-rich samples (Omotoso et al. 2006). In this method the total dioctahedral Al-rich 2:1 layer clay (illite, muscovite, dioctahedral Al- and Al+Mg-smectite, mixed-layered illite-smectite) are quantified together by careful fitting of the 060 reflection (Środoń et al. 2001) and are referred to as the illite+smectite group. The structural details of the clay minerals that form this group are precisely identified and quantified using the XRD patterns

of oriented preparations of the <2 µm grain size fractions and the multi-specimen computer simulation method (e.g. Sakharov et al. 1999; McCarty et al. 2009).

Clay mineral composition was investigated in <2 µm equivalent spherical diameter fractions, separated from selected natural samples after chemical purification and centrifugation including carbonate removal, organic matter (OM) oxidation, and Fe-(oxy-)-hydroxides removal (Jackson 1969). Diffraction data were collected from oriented preparations of the Ca-exchanged clay fractions in both the air-dry state and after saturation with ethylene glycol (EG). Qualitative and quantitative analyses were performed by full XRD pattern simulation using Sybilla software (Chevron proprietary, cf. McCarty et al. 2008), using the formalism described by Drits and Tchoubar (1990).

The chemical composition of the selected opal-rich, clay-poor samples (Table 1a) was analyzed with the common inductively coupled plasma-optical emission

spectroscopy (ICP/OES), LiBO<sub>3</sub>-fusion method, by Activation Laboratories Ltd., Ancaster, Ontario, Canada. Total organic carbon (TOC) was determined using a LECO elemental analyzer.

## RESULTS

### Bulk samples from the Monterey Formation

Natural samples were found to consist of four different mineral groups: (1) coarse detrital minerals (quartz > plagioclase > K-feldspar); (2) clay minerals (illite+smectite group >> kaolinite); (3) biogenic opal-A and -CT with minor opal-C; and (4) carbonate minerals either as cement (<10 wt%) or as carbonate

**TABLE 1A.** Mineral and chemical composition, in wt%, CEC (in meq/100 g), and mass loss at 200 °C (in wt%) of selected opal-rich, clay-poor samples from the Monterey Formation

Sample	Quartz	K-feldspar	Plagioclase	Total carbonate <sup>a</sup>	Pyrite	Opal -A	Opal -CT	Illite+smectite group	CEC	H <sub>2</sub> O200	Total organic C	SiO <sub>2</sub>	Al <sub>2</sub> O <sub>3</sub>	Fe <sub>2</sub> O <sub>3</sub>	MgO	CaO	Na <sub>2</sub> O	K <sub>2</sub> O	TiO <sub>2</sub>	P <sub>2</sub> O <sub>5</sub>	LOI
A max 1	2.0	1.0	1.0	0.0	1.0	89	1	2.0	7.3	2.4	1.55	84.81	2.08	1.14	0.24	0.35	0.98 <sup>H1</sup>	0.32	0.1	0.1	9.56
CT max 1	3.0	0.5	1.5	0.0	0.3	0	91	3.0	11.7	3.8											
CT max 2	4.0	1.0	3.5	0.5	0.5	0	87	4.0	12.2	3.9	1.35	81.11	4.49	1.49	0.47	0.68	1.14	0.81	0.20	0.14	9.08
CT max 3	4.0	1.5	2.7	0.2	0.6	0	85	5.0	9.0	2.4	1.51	82.84	3.09	1.40	0.23	0.41	0.85	0.55	0.13	0.08	7.47
CT max 4	2.4	0.5	2.5	0.0	1.0	0	89	4.5	10.4	3.4	1.40	81.95	3.15	1.42	0.29	0.37	0.93	0.6	0.16	0.1	9.01
CT max 5	3.5	2.0	4.4	0.2	1.5	0	80	8.0	10.1	3.3		79.65	4.28	3.57	0.45	0.59	1.07 <sup>H2</sup>	0.73	0.21	0.17	10.53
CT max 6	2.0	0.5	2.0	0.0	0.9	0	90	3.5	11.0	3.5	1.99	84.49	2.85	0.50	0.21	0.33	0.79	0.42	0.12	0.1	8.55
CT max 7	2.0	1.0	2.0	3.5	0.7	0	85	5.0	9.2	2.8	1.20	84.67	2.11	0.63	0.85	1.49	0.65	0.35	0.08	0.11	8.92
CT max 8	3.5	1.2	3.8	0.0	0.9	0	86	4.0	12.4	3.0	1.15	82.83	3.46	1.10	0.29	0.47	0.97	0.61	0.16	0.14	10
CT max 9	2.0	0.5	1.5	0.4	0.7	1	88	5.0	11.6	3.1	0.88	85.31	2.48	0.89	0.25	0.59	0.81	0.4	0.10	0.08	9.43
CT max 10	3.5	2.0	3.0	0.2	0.6	1	83	6.0	14.1		1.90	85.33	3.21	0.92	0.25	0.37	0.86	0.53	0.14	0.09	8.47
CT max 11	1.5	0.5	1.0	4.4	0.6	0	88	3.5	12.0		1.19	83.95	2.37	0.87	1.03	1.68	0.59	0.3	0.09	0.11	9.88

<sup>a</sup> Mostly excess-Ca dolomite, with traces of calcite; <sup>H1</sup> 0.9% of halite <sup>H2</sup> 0.4% of halite.

**TABLE 1B.** Opal-assigned CEC and the excess element and ion concentrations calculated by subtracting contributions of individual mineral species to the total element concentrations in the bulk rock, using the I-S model of the illite+smectite mineral

Sample	I-S model excess element concentration (wt%)							I-S model excess ion (meq/100 g)					Excess (opal)		Excess (opal)	
	K	Al	Mg	Ca	Na	Fe	K <sup>+</sup>	Na <sup>+</sup>	Mg <sup>2+</sup>	Ca <sup>2+</sup>	(AlO <sub>2</sub> ) <sup>-</sup>	(Fe <sup>3+</sup> O <sub>2</sub> ) <sup>-</sup>	CEC (meq/100 g)	H <sub>2</sub> O200 (wt%)		
A max 1	0.06	0.58	0.11	0.22	0.28	0.31	1.6	12.0	9.4	11.0	21.6	5.6	6.8		2.53	
CT max 1													10.9		3.90	
CT max 2	0.41	1.29	0.16	0.30	0.53	0.76	10.5	22.9	13.4	14.8	47.8	13.6	11.3		4.14	
CT max 3	0.09	0.42	0.04	0.17	0.36	0.65	2.4	15.9	3.3	8.5	15.6	11.6	7.1		2.45	
CT max 4	0.29	0.65	0.11	0.19	0.44	0.48	7.5	19.4	8.8	9.7	24.0	8.7	8.6		3.49	
CT max 5	0.08	0.35	0.13	0.25	0.21	1.72	2.1	9.0	10.5	12.6	13.0	30.7	6.7		3.41	
CT max 6	0.17	0.70	0.07	0.18	0.39	-0.10	4.4	17.0	6.1	9.0	25.9	0.0	9.9		3.65	
CT max 7	0.00	0.02	0.02	-0.01	0.27	0.03	0.0	11.8	1.5	0.0	0.7	0.5	7.2		2.86	
CT max 8	0.21	0.69	0.11	0.26	0.38	0.31	5.5	16.3	9.5	12.9	25.7	5.6	11.6		3.18	
CT max 9	0.11	0.31	0.03	0.14	0.43	0.24	2.8	18.7	2.3	7.2	11.6	4.3	9.7		3.03	
CT max 10	-0.03	0.24	0.04	0.13	0.34	0.31	0.0	14.7	3.0	6.4	9.1	5.5	12.5			
CT max 11	0.07	0.55	0.04	0.14	0.32	0.25	1.9	14.0	3.4	7.2	20.2	4.5	11.3			

Notes: Excess element concentrations calculated from the bulk contents corrected for the element contributions from: K-feldspar (K = 14.3%, Al = 9.7%, Na = 1%), plagioclase (Ca = 1%, Na = 8%, Al = 10%), excess-Ca dolomite (Fe = 1%, Ca = 23%, Mg = 12%), pyrite (Fe = 46.5%), halite (Na = 39%); illite+smectite group considered as I-S (K = 3%, Al = 16%, Mg = 1.5%, Ca = 1%, Na = 1%, Fe = 1%) or montmorillonite (Al = 9%, Mg = 2.5%, Ca = 2%, Na = 2%, Fe = 3%). Excess (opal) CEC and excess (opal) H<sub>2</sub>O200 calculated by subtracting the illite+smectite contribution to measured bulk rock CEC and H<sub>2</sub>O200, using 60 meq/100 g and 7 wt% for I-S model and 100 meq/100 and 14 wt% for montmorillonite model, respectively, and normalizing to the opal content. Excess element concentration less than zero was approximated by zero.

**TABLE 1C.** Opal-assigned CEC and the excess element and ion concentrations calculated by subtracting contributions of individual mineral species to the total element concentrations in the bulk rock, using the montmorillonite model of the illite+smectite mineral

Sample	Montmorillonite model excess element concentration (wt%)							Montmorillonite model excess ion (meq/100 g)					Excess (opal)		Excess (opal)	
	K	Al	Mg	Ca	Na	Fe	K <sup>+</sup>	Na <sup>+</sup>	Mg <sup>2+</sup>	Ca <sup>2+</sup>	(AlO <sub>2</sub> ) <sup>-</sup>	(Fe <sup>3+</sup> O <sub>2</sub> ) <sup>-</sup>	CEC (meq/100 g)	H <sub>2</sub> O200 (wt%)		
A max 1	0.12	0.72	0.09	0.20	0.26	0.27	3.1	11.1	7.8	10.0	26.8	4.9	5.9		2.38	
CT max 1													9.5		3.67	
CT max 2	0.53	1.57	0.12	0.26	0.49	0.68	13.6	21.1	10.2	12.8	58.2	12.2	9.4		3.81	
CT max 3	0.24	0.77	-0.01	0.12	0.31	0.55	6.2	13.7	0.0	6.0	28.5	9.8	4.7		2.03	
CT max 4	0.43	0.96	0.06	0.15	0.40	0.39	10.9	17.4	5.1	7.5	35.7	7.1	6.6		3.14	
CT max 5	0.32	0.91	0.05	0.17	0.13	1.56	8.2	5.5	3.9	8.6	33.8	27.8	2.6		2.71	
CT max 6	0.28	0.94	0.04	0.15	0.36	-0.17	7.1	15.5	3.2	7.3	35.0	0.0	8.3		3.38	
CT max 7	0.15	0.37	-0.03	-0.06	0.22	-0.07	3.8	9.7	0.0	0.0	13.7	0.0	4.9		2.44	
CT max 8	0.33	0.97	0.07	0.22	0.34	0.23	8.6	14.6	6.2	10.9	36.1	4.2	9.8		2.85	
CT max 9	0.26	0.66	-0.02	0.09	0.38	0.14	6.7	16.6	0.0	4.7	24.6	2.5	7.4		2.63	
CT max 10	0.15	0.66	-0.02	0.07	0.28	0.19	3.9	12.1	0.0	3.4	24.6	3.3	9.6			
CT max 11	0.18	0.79	0.01	0.11	0.29	0.18	4.6	12.5	0.5	5.4	29.3	3.3	9.7			

Notes: For calculation details see footnote below Table 1b.

beds with higher carbonate contents. The samples represent a range of opal content from zero to more than 90% (median 48%), and from 0 to 27% of total clay minerals content (Figs. 1 and 2) with a median of 12% for the illite+smectite group.

Due to potential variability of the opal and the I-S properties in the diagenetic zones of opal-A and opal-CT, the database of natural samples was divided into two roughly equal groups, based on the dominant opal type ("opal-A zone" and "opal-CT zone"). In these sample subsets the minor opal type is  $\leq 5$  wt%. The CEC values measured in these zones vary from  $<2$  meq/100 g to 17.3 meq/100 g in the opal-A zone, and from  $<2$  meq/100 g to 25.9 meq/100 g in the opal-CT zone.  $H_2O_{200}$  values vary from 0.1 to 3.9 and to 4.1 wt%, respectively (Figs. 1 and 2).

The quantitative relationships between CEC or  $H_2O_{200}$  content and wt% of the two components that can provide bulk rock CEC and  $H_2O_{200}$ , i.e., opal and illite+smectite groups are similar for rocks with opal-A and opal-CT (Figs. 1 and 2). There is no statistically significant linear correlation between neither CEC nor  $H_2O_{200}$  content and illite+smectite, but a very weak positive relationship can be observed between CEC and illite+smectite. The relationship between CEC and opal content has a clear, though scattered concave shape, while that for  $H_2O_{200}$  and opal content is linear, positive and less scattered, with a slight concave shape, especially for the opal-A samples.

The scattered, co-varying increase of illite+smectite mineral content with opal content up to  $\sim 30\%$  (Opal-A zone) and to  $\sim 50\%$  (Opal-CT zone) shown in Figure 3 suggests that opal controls CEC in samples with low opal content (Figs. 1 and 2).

The illite+smectite vs. opal relationships are also similar to the concave shapes of the CEC vs. opal relationships (compare Figs. 1 and 2 with Fig. 3). Unless assuming that opal CEC is high in the samples with low opal content and it is much lower in the opal-rich samples, the similarity of these concave relationships suggests that illite+smectite content rather than opal is dominating bulk CEC in the majority of the samples. The samples with intermediate opal content have the highest illite+smectite content and, therefore, the highest CEC. These relationships demonstrate that CEC and  $H_2O_{200}$  are controlled by different factors; CEC being more influenced by illite+smectite content and  $H_2O_{200}$  more by opal content. The concave shaped relationship of illite+smectite vs. opal content is due to primary deposition and not alteration because it exists across the opal-A and opal-CT diagenetic transition.

A third subset of natural samples that contain at least 85% opal-A and  $\leq 5\%$  illite+smectite was selected from the database (11 opal-CT samples and 1 opal-A sample, Table 1). These samples can be considered as almost pure standards, where the measured bulk CEC and  $H_2O_{200}$  are negligibly affected by non-opal minerals. The opal-CT samples have CEC variability from 9.0 to 14.1 meq/100 g (median 11.6 meq/100 g) and  $H_2O_{200}$  values from 2.4 to 3.9% (median 3.3%). The opal-A sample has a CEC of 7.4 meq/100 g and 2.4% of  $H_2O_{200}$ . Due to difficulty in the quantification of disordered phases in an amorphous matrix, and the problem with determination of minerals with variable crystal chemistry, a careful quantification of minerals in the subset of the 12 opal-rich samples was repeated using various

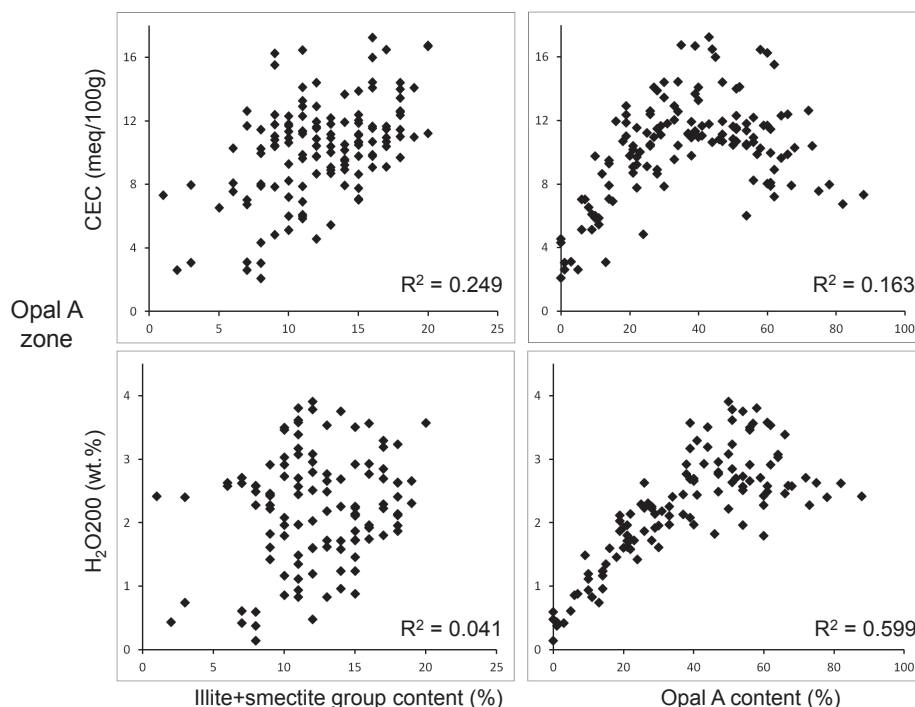


**FIGURE 1.** Relationships between opal-A content, illite+smectite mineral group content, and the bulk rock cation exchange capacity (CEC), and mass of water desorbed at 200 °C ( $H_2O_{200}$ ) in samples collected from the Monterey Formation, California. Presented are samples rich in opal-A (opal-A zone). Linear correlation coefficient  $R^2$  is given for the Model I regression  $y = ax + b$ .

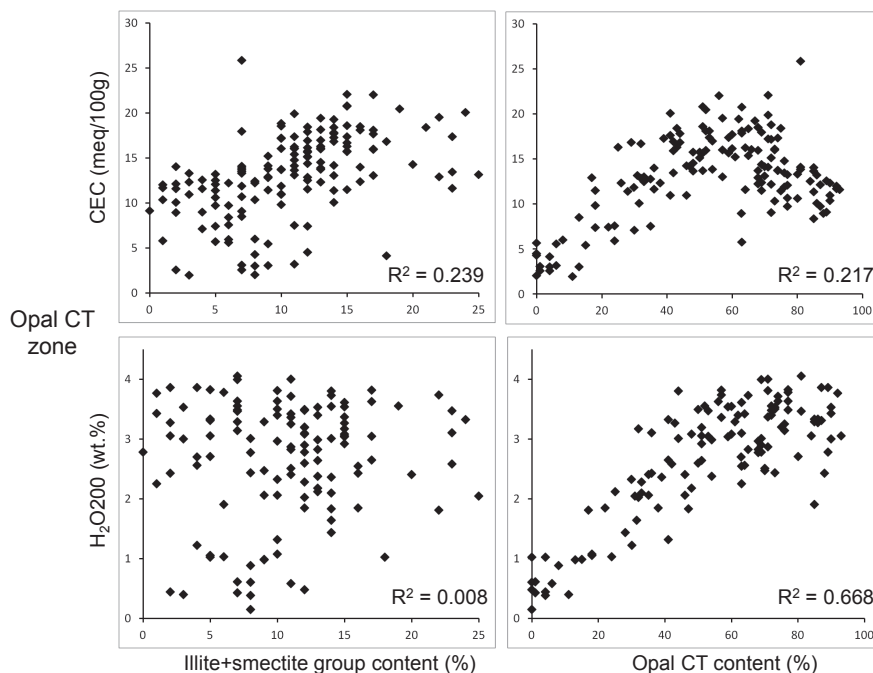


**FIGURE 2.** Relationships between opal-CT content, illite+smectite mineral group content, and the bulk rock cation exchange capacity (CEC), and mass of water desorbed at 200 °C ( $H_2O_{200}$ ) in samples collected from the Monterey Formation, California. Presented are samples rich in opal-CT (opal-CT zone).  $R^2$  as in Figure 1.

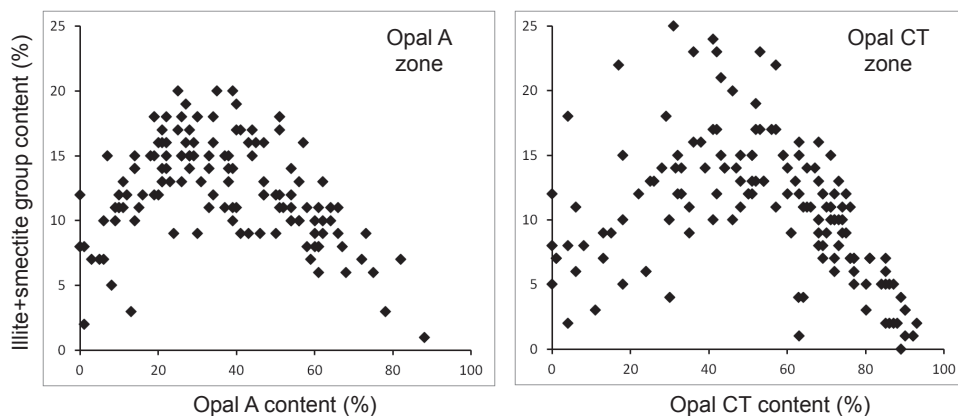


**FIGURE 3.** Mineral relationships between opal-A (left) and opal-CT (right) content, and illite+smectite mineral group content for samples collected in the Monterey Formation, California, shown separately for opal-A and opal-CT zones.

mineral standards, which were different than those used for the quantification of the majority of Monterey Formation samples. At low mineral contents, the relative quantification error is usually high. The aim of the additional analysis was to find the highest acceptable content of minerals other than opal, to account for the chemical composition of the opal-rich samples. This procedure resulted in an increase in feldspar and carbonate contents by roughly 1% with respect to the previous quantification of the entire rock series, while illite+smectite content increased by 2–4%, which is consistent with the assumed quantification errors. At such low concentrations the composition of the illite+smectite group cannot be determined in XRD patterns from bulk samples. Only a discrete illite component was identified in some samples

from sharp peaks close to 1 nm.

The composition of the <2  $\mu m$  clay mineral fraction is similar in all samples, regardless the opal species. The samples have two types of mixed-layered illite-smectite, one with random interstratification (R0) and up to 19% of illite layers, and the other with ordered interstratification (R1) and 70–80% of illite layers. The discrete illite and kaolinite contents vary from 6 to 17%, accompanied by a few percent chlorite (Fig. 4).

#### Opal mineral standards

Three opal-A standards from different locations have CEC values from 3.5 to 6.0 meq/100 g, in the following order: opal-A 586 > opal-A 282 >> opal-A 252. The lowest CEC among the



opal-A samples is equal to that recorded for the opal-CT standard (3.6 meq/100 g). Opal-C has 1.3 meq/100 g, which is close to the CEC measurement limit, while the tridymite and obsidian samples have CEC values <1 meq/100 g (Table 2).

Water loss at 110 and 200 °C in the opal samples does not follow the same order as the CEC values. The opal-CT H<sub>2</sub>O110 of 1.5% is close to the lowest value for the opal-A range (1.7–3.2%). There is a significant variability in the opal-A H<sub>2</sub>O200 values, from 3.5 to 5.3%. In the opal-C, tridymite, and obsidian samples, the H<sub>2</sub>O110 and H<sub>2</sub>O200 values are low, ≤0.6 wt%.

The TG patterns of the opal-A and -CT standards have qualitatively similar features and can be divided into temperature ranges that correspond to different reactions. The first reaction seems to occur between room temperature and 300 °C, and the second reaction is completed at about 650 °C (Fig. 5). Therefore, these two temperatures were chosen as reference values for mass loss determination, TG-300 and TG-650, respectively, along with the final mass loss value at 1000 °C, TG-1000 (Table 2).

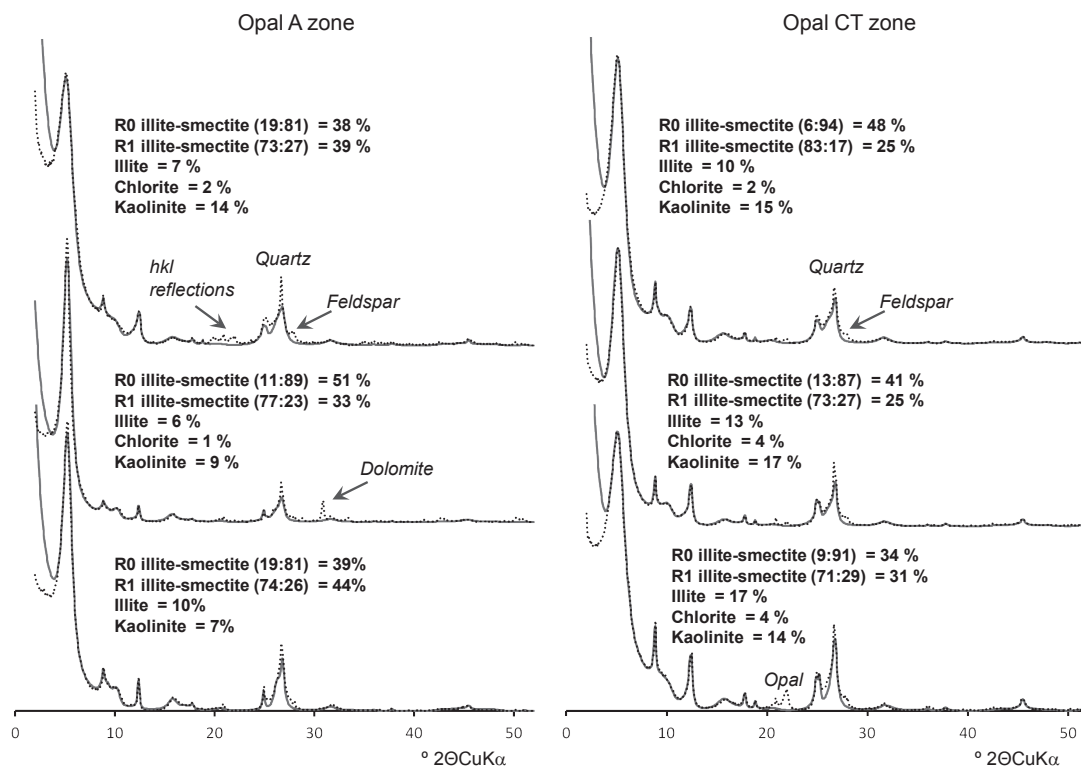
The total TG mass loss of the opal-A and -CT standards follow the same order of mass loss determined from H<sub>2</sub>O110 and H<sub>2</sub>O200 analyses with the moisture balance: opal-A 586 > opal-A 252 >> opal-A 282 > opal-CT 417 (Table 2). The final mass loss ranges for opal-A and -CT are from 7.1 to 15.1%. However, in addition to H<sub>2</sub>O removal (mass 18), the evolved gas MS signal also showed the release of CO<sub>2</sub> (mass 44) in the temperature range of ~450–650 °C. Therefore, the estimated range of maximum H<sub>2</sub>O and OH loss in the opal-A and -CT standards, derived from

the TG-1000 values, has been reduced to 6–12%, which is close to the loss of ignition (LOI) range measured for the opal-rich samples from the Monterey Formation (Table 1a), corrected for organic carbon (TOC) and the carbonate mineral CO<sub>2</sub> content. The CO<sub>2</sub> evolved from the opal standards probably comes from organic matter because temperature interval is lower than that for carbonate minerals, which were also not identified by XRD in the opal standards. The opal-C, tridymite, and obsidian standards have negligible mass loss during TG analysis, only <0.5 wt% at TG-650 and maximum 0.85 wt% at TG-1000, consistent with the mass loss determined with the moisture analyzer (Table 2).

### Modeling the opal CEC and H<sub>2</sub>O200 in sedimentary basins

The illite+smectite and opal phases are the main contributors to the CEC and H<sub>2</sub>O200 in the sample set studied. Because illite+smectite CEC can be well constrained from the structural analysis (Środoń 2009; Środoń et al. 2009), it can serve as independent verification for the modeling applied to estimate the corresponding CEC values for opal and illite+smectite.

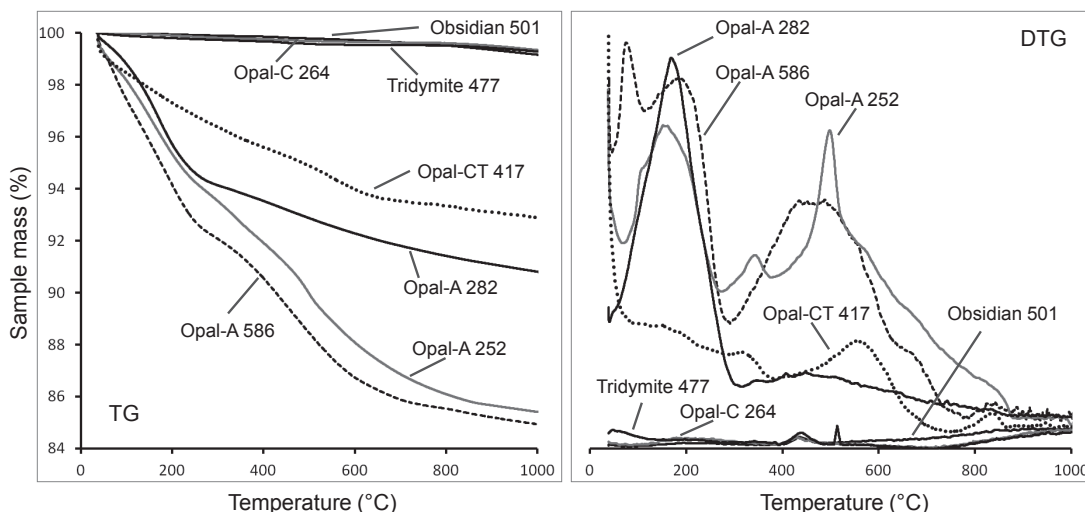
The error minimization ( $F_{\min}$ ) approach, using the least-squares-based calculation was applied. This method uses as the criterion of optimization, the lowest difference between the bulk rock measured (CEC<sub>meas</sub>, H<sub>2</sub>O200<sub>meas</sub>) and modeled (CEC<sub>model</sub>, H<sub>2</sub>O200<sub>model</sub>) values for individual samples. The multi-variable linear regression model used in simultaneously solving multiple equations in the sample set is



**FIGURE 4.** X-ray diffraction patterns of oriented specimens of clay fractions (<2 μm), separated from the Monterey Formation samples, Ca-exchanged and saturated with ethylene glycol (black dotted line). Mineral structures determination and quantification was performed based on the XRD pattern modeling (gray solid line).

**TABLE 2.** Cation exchange capacity and mass loss of mineral standards during moisture analysis tests and thermogravimetry analysis

Sample	Moisture analysis (H <sub>2</sub> O loss at given temperature)		CEC (meq/100 g)	TG analysis (mass loss at given temperature)			Sample origin
	H <sub>2</sub> O110 (%)	H <sub>2</sub> O200 (%)		H <sub>2</sub> OTG300 (%)	H <sub>2</sub> OTG650 (%)	H <sub>2</sub> OTG1000 (%)	
Opal-A 282	1.67	3.49	5.6	5.98	8.09	9.19	Santa Barbara Co., California, U.S.A.
Opal-A 586	3.20	5.34	6.0	7.94	13.75	15.07	Auvergne, France
Opal-A 252	3.17	4.09	3.5	6.49	12.60	14.59	Monterey Formation, California, U.S.A.
Opal-CT 417	1.48		3.6	3.63	6.34	7.11	Jalisco, Mexico
Opal-C 264	<0.05	<0.05	1.3	0.19	0.37	0.67	Virgin Valley, Humboldt Co., Nevada, U.S.A.
Tridymite 477	0.56		0.5	0.28	0.48	0.72	Germany (detailed location unknown)
Obsidian 501	0.18	0.32	0.8	0.11	0.32	0.85	Millard City, Utah, U.S.A.

**FIGURE 5.** Patterns of thermogravimetric (TG) analysis performed on the mineral standards (**left**). The same analyses presented in a form of first derivative TG patterns (DTG; **right**).

$$F_{\min} = \sum_n \left[ \left( \text{CEC}_{\text{meas}} - \text{CEC}_{\text{model}} \right)^2 + \left( \text{H}_2\text{O}200_{\text{meas}} - \text{H}_2\text{O}200_{\text{model}} \right)^2 \right] \quad (1)$$

and

$$\text{CEC}_{\text{model}} = \frac{(\text{CEC}_{\text{opal}} \times W_{\text{opal}} + \text{CEC}_{\text{I+S}} \times W_{\text{I+S}})}{100} \quad (2a)$$

and

$$\text{H}_2\text{O}200_{\text{model}} = \frac{(\text{H}_2\text{O}200_{\text{opal}} \times W_{\text{opal}} + \text{H}_2\text{O}200_{\text{I+S}} \times W_{\text{I+S}})}{100} \quad (2b)$$

where  $n$  is a number of samples (equations) solved simultaneously in a model calculation where  $\text{CEC}_{\text{opal}}$ ,  $\text{H}_2\text{O}200_{\text{opal}}$ ,  $\text{CEC}_{\text{I+S}}$ , and  $\text{H}_2\text{O}200_{\text{I+S}}$  are the unknown values undergoing optimization. These variables are assumed to be constant in this calculation over the entire data set, while  $W_{\text{opal}}$  and  $W_{\text{I+S}}$  are the known contents of the opal and illite+smectite mineral group in wt%. The mineral quantification error can be as high as  $\pm 3$  wt% absolute for opals, due to their disordered structure, while it is up to  $\pm 2\%$  absolute for the illite+smectite mineral group (Omotoso et al. 2006). The CEC measurement error was considered as  $\pm 1$  meq/100 g (Derkowski and Bristow 2012), while the repeatability of  $\text{H}_2\text{O}200$  was determined to be  $\pm 0.1\%$  with the moisture analyzer. For each sample, the  $\text{CEC}_{\text{meas}}$ ,  $\text{H}_2\text{O}200_{\text{meas}}$ ,  $W_{\text{opal}}$ , and  $W_{\text{I+S}}$  values were allowed to vary within these measurement error

limits. The adjusted  $W_{\text{opal}}$  and  $W_{\text{I+S}}$  mineral contents, and the adjusted  $\text{CEC}_{\text{meas}}$  and  $\text{H}_2\text{O}200_{\text{meas}}$  values were thus fitted within the given maximum error to Equations 2a and 2b to minimize the  $F_{\min}$  (Eq. 1) simultaneously, using the non-linear Solver engine (Frontline Systems Co., Incline Village, Nevada, U.S.A.).

The best fit between the measured and modeled bulk rock CEC values (Eqs. 1 and 2a), with the Pearson correlation coefficient  $R^2 = 0.822$ , was found in the opal-A zone for  $\text{CEC}_{\text{I+S}}$  of 59.7 meq/100 g and opal-A CEC value of 8.1 meq/100 g. In the opal-CT zone the highest correlation coefficient ( $R^2 = 0.857$ ) was determined for  $\text{CEC}_{\text{I+S}}$  of 57.8 meq/100 g and opal-CT CEC value of 13.3 meq/100 g (Fig. 6). The calculated end-member  $\text{H}_2\text{O}200$  values ( $\text{H}_2\text{O}200_{\text{opal}}$ ) that give the best fit between the measured and modeled bulk rock  $\text{H}_2\text{O}200$  values (Eqs. 1 and 2b) are 3.40% for opal-A ( $R^2 = 0.848$ ) and 3.68% for opal-CT ( $R^2 = 0.881$ ; Fig. 6). The calculated  $\text{CEC}_{\text{opal}}$  and  $\text{H}_2\text{O}200_{\text{opal}}$  values of both opals (A and CT) remain within the ranges determined for almost pure opal samples from the Monterey Formation (Tables 1b and 1c), confirming validity of the model.

Careful simulation of the XRD patterns from the  $< 2 \mu\text{m}$  clay fractions following the approach by McCarty et al. (2008, 2009), revealed that the samples from both opal-A and opal-CT zones contain a mixture of I-S phases, R0 and R1 in roughly equal proportions, regardless the sample depth. This finding is different from the results by Compton (1991) who assigned the occurrence of R1 ordering in I-S to opal-CT/quartz diagenetic

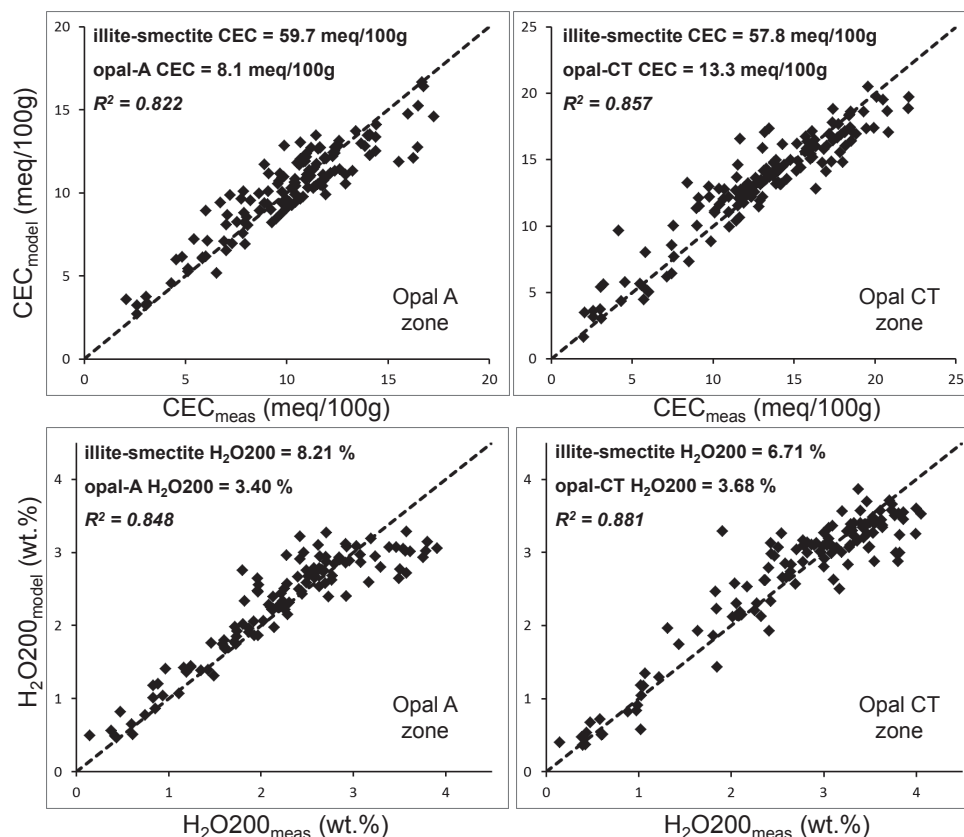


**FIGURE 6.** Results of multiple linear correlation modeling (Eqs. 1 and 2) for CEC and  $H_2O_{200}$  performed separately for opal-A zone and opal-CT zones as a correlation between the measured bulk rock data ( $CEC_{meas}$ ,  $H_2O_{200,meas}$ ) and the modeled values ( $CEC_{model}$ ,  $H_2O_{200,model}$ ).  $R^2$  denotes the correlation coefficient.

transition, not seen in the opal-A zone. Due to the independence of the degree of the opal diagenesis, here the I-S R0 and R1 phases are interpreted as being of detrital origin that have not undergone illitization. The temperature of opal-A to opal-CT transition is broadly accepted as 35–50 °C, which is lower than the onset of illitization (Keller and Isaacs 1985; Compton 1991; Huang et al. 1993). For the Monterey Formation, an even lower temperature of 17 to 21 °C was suggested for opal-A to opal-CT transition (Matheny and Knauth 1993).

The CEC of the total illite+smectite group (average for illite and different I-S populations) calculated from the composition of clay fractions varies within a narrow range of 53–67 meq/100 g assuming an average 110 meq/100 g for the smectite component in I-S and 15 meq/100 g of CEC for the non-expandable illite layers (Fig. 4). The  $CEC_{I+S}$  values calculated using Equation 2a are exactly within the CEC range for illite+smectite group found from the clay fractions, which provides independent evidence that the real  $CEC_{I+S}$  values cannot be significantly different than the calculated  $CEC_{I+S}$ . Therefore, to match the measured bulk rock CEC, the CEC of opal in the Monterey Formation samples also cannot be much different than the calculated  $CEC_{opal}$  values. Moreover, the  $CEC_{I+S}$  calculated independently for the opal-A zone and the opal-CT zone have essentially the same values with an insignificant difference, which provides additional validity for the models.

Additional confirmation of the modeling accuracy is that the modeled values for opal and illite+smectite explain the concave shape of the CEC vs. opal content curve (Fig. 7). A simulation exercise was performed to verify the CEC vs. opal content prediction model. The  $H_2O_{200}$  part was excluded from Equation 1. In two independent simulations the  $CEC_{opal}$  value in Equation 2a was fixed at 0 or 20 meq/100 g, which is approximately twice the calculated  $CEC_{opal}$  value, and the simulations were performed again to find the lowest  $F_{min}$ . The third model with unconstrained  $CEC_{opal}$ , however, returned the  $CEC_{opal}$  and  $CEC_{I+S}$  values exactly the same as given by the models involving the  $H_2O_{200}$  part of the Equation 1 (Fig. 6), reproducing perfectly the concave shape of CEC-opal relationship. In both tested combinations with the constrained  $CEC_{opal}$ , the  $R^2$  correlation coefficient was significantly worse and the concave shape of CEC vs. opal content was either not reproduced or followed with a much lower quality of fit (Fig. 7). For these two simulations, the calculated  $CEC_{I+S}$  values moved far beyond the range estimated from the clay fraction analysis, and corresponded to pure smectite when  $CEC_{opal}$  was fixed at zero or to an almost pure illite when  $CEC_{opal}$  was set to 20 meq/100 g (Fig. 7). Therefore, the realistic range of  $CEC_{opal}$  values in the Monterey Formation must be much narrower than 0–20 meq/100 g.

The calculated end-member  $H_2O_{200}$  values for the illite+smectite group ( $H_2O_{200,I+S}$ ) are 8.21% in the opal-A zone



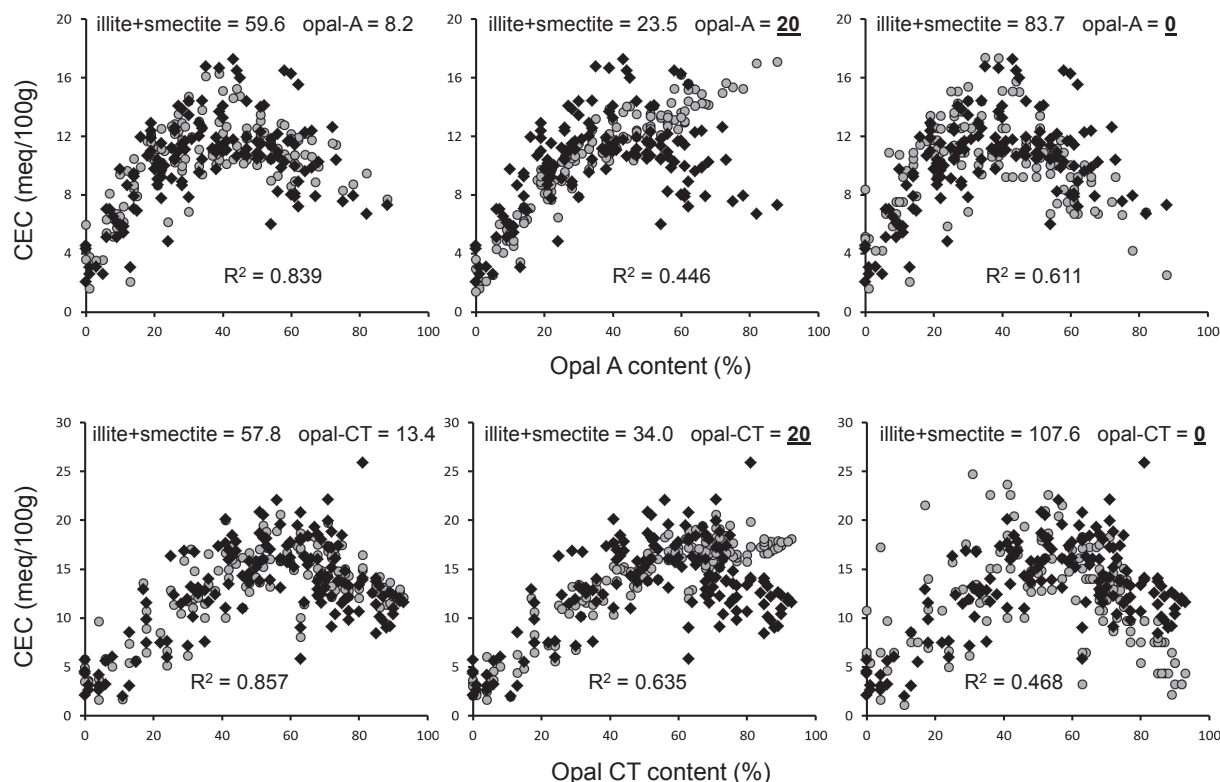


**FIGURE 7.** Bulk rock opal content vs. CEC values measured and modeled with multiple linear correlation models (Eqs. 1 and 2a). Left = unconstrained  $CEC_{opal}$  and  $CEC_{I+S}$  values; middle and right = fixed value of  $CEC_{opal} = 20$  and  $0$  meq/100 g, respectively. Fixed parameters are shown in bold and underlined. Black diamonds = measured values, gray circles = modeled values. Linear correlation coefficient  $R^2$  given for the Model I regression between the measured and modeled CECs.

and 6.71% in the opal-CT zone. Pure smectite equilibrated at 47% RH and heated at 200 °C releases on average 16.0 wt% of adsorbed water when Ca-exchanged and ~11.3% when Na-exchanged (Środoń and McCarty 2008); the same measurement conditions were applied for  $H_2O_{200}$  measurement in this study. The composition of exchangeable cations in the Monterey samples is unknown, but can be assumed to be a mixture of Na and Ca. Because the separated clay fraction has an ~50% equivalent smectite layer content in the total illite + illite-smectite (R1 and R0) minerals, the modeled  $H_2O_{200_{I+S}}$  values (6.7–8.2 wt%) match perfectly the values measured by Środoń and McCarty (2008).

## DISCUSSION

### Surface charge in biogenic opals from the Monterey Formation

Comparing the chemical and mineral composition of the 12 opal-rich samples provides an independent approach to evaluating the composition and surface properties of the opal species. Even if the maximum realistic non-opal mineral contents are used, the chemical composition does not match the mineral composition of the opal-rich samples (Table 1) if the opal fraction quantified by XRD is considered as pure  $SiO_2 + H_2O$ .

Two chemical models were considered; assuming that the illite+smectite mineral quantified in the opal standards has a pure montmorillonite composition (average value from Środoń and

McCarty 2008), or it is the I-S with ~50%S, as estimated from the detailed clay analysis (Fig. 4) and the  $CEC_{I+S}$  model (Fig. 6). The I-S with ~50%S and a pure montmorillonite have different average chemical compositions, so they in turn contribute differently to the bulk rock element concentrations. For both applied models, after subtracting the contributions of all identified and quantified mineral species other than opal to the total element concentrations in the bulk rock, the excess K, Na, Al, Fe, Ca, and Mg are observed in almost all samples analyzed (only Fe for one sample is slightly underestimated, Tables 1b and 1c). The excess Al reaches up to >1.0% while the average excess Na exceeds 0.3%. Assuming the negligible contribution from closed pore fluids, the excess element concentrations represent impurities in the opal silica network. If this model is correct, Al substitutes for Si and provides the negative net charge of silica while  $Na^+$ ,  $Ca^{2+}$ ,  $Mg^{2+}$ , and  $K^+$  are then the compensating cations (Webb and Finlayson 1987; Gehlen et al. 2002; Gaillou et al. 2008). The valence of Fe in the studied samples is unknown. It is accepted that  $Fe^{3+}$  can behave like Al and substitute for Si (Rondeau et al. 2012). Alternatively, Fe may occur as separate, amorphous, XRD-undetectable oxy-hydroxide phase or linked to organic matter (Van Bennekom and van der Gaast 1976). Charge balance in the opal structure can be compared by assuming that the excess  $(AlO_2)^-$  and  $(Fe^{3+}O_2)^-$  are the species providing the negative charge excess in the silica network, and

the monovalent and divalent cations compensate this negative charge (Tables 1b and 1c, Fig. 8). The charge balance tested with two different element excess sets of anions (from sole Al or total Al +  $\text{Fe}^{3+}$ ) and the total cations, determined from two different illite+smectite mineral models (montmorillonite or I-S) shows a close qualitative match (Fig. 8), which supports the model used. Despite good linear correlation, the models assuming total Al and  $\text{Fe}^{3+}$  substitution in the silica framework have a significant deviation from the zero charge balance, with a trend line slope  $\ll 1$  for both mineral models. When assuming only Al substitution for Si (Gehlen et al. 2002; Koning et al. 2007; Gaillou et al. 2008), the charge balance fit becomes perfect 1:1 for the montmorillonite model, while the I-S model trend line displays a noticeable intercept of excess positive charge (Fig. 8). The calculation, therefore, suggests that Fe occurs outside the opal structure as suggested by Van Bennekom and van der Gaast (1976), the minor quantities of illite+smectite mineral is represented mostly by smectite, and the silica network contains abundant Al substitutions compensated by common seawater cations: Na, Ca, Mg, and K.

The bulk CEC measured for the opal-rich samples (Table 1a) can be reduced by the CEC of re-quantified, maximum possible illite+smectite content, using either the I-S model ( $\sim 60$  meq/100 g) or the montmorillonite model (100 meq/100 g), in the same manner as calculating the excess element concentrations. These “excess CEC” values, when normalized to the opal content, represent the estimated CEC of pure opal, which—assuming the illite+smectite mineral admixture as smectite—vary within 3–10 meq/100 g (Table 1c). These values are consistent with CEC measured for the pure opal standards (Table 2). The  $\text{CEC}_{\text{opal}}$  values modeled for opal-A and opal-CT using the entire set of  $\sim 300$  samples from the Monterey Formation (Fig.

6) need to be decreased by the CEC equivalent of 2–4 wt% of smectite that the selected opal-rich samples revealed after careful re-analysis (Table 1a). This brings the modeled  $\text{CEC}_{\text{opal}}$  values down to the range of 4–11 meq/100 g, as in the opal CEC range computed for the set of the 12 opal-richest samples (Table 1c).

The CEC of the pure virtual opal accounts for only  $\sim 10$ –50% of the total opal charge determined from Al substitution for Si (compare Tables 1b and 1c). The mismatch between the CEC and the total opal charge can be explained by distinguishing between the external (exchangeable) and internal (fixed) compensating cations (cf. Robertson and Twedily 1953; Flörke et al. 2012) in a similar way as performed for OH groups and Si-substituting cations by Webb and Finlayson (1987) and Loucaides et al. (2010). The hexamminecobalt cation used to measure CEC in this study is a large complex cation that does not enter micropores with a sub-nanometer effective size dimension (Derkowski et al. 2006). If smaller cations were applied for the CEC determination, more total compensating cations should be exchanged in the silica structure, as showed by Robertson and Twedily (1953). Using ammonia method those authors found CEC of pure opal samples in the range of 31–54 meq/100 g comparing to 8–12 meq/100 g determined with a large methylene blue molecule. The range of CEC determined with a large hexamminecobalt(III) cation and the total CEC estimated from excess ion based on chemical composition (Table 1c; Fig. 8) perfectly match the ranges given by Robertson and Twedily (1953).

#### Opal chemical composition and smectite authigenesis

Smectite rather than detrital I-S particles embedded in the Monterey Formation opal structure should not be surprising. Van Bennekom and van der Gaast (1976), Badaut and Risacher (1983), Michalopoulos et al. (2000), and Gehlen et al. (2002) independently suggested the formation of very fine phyllo-

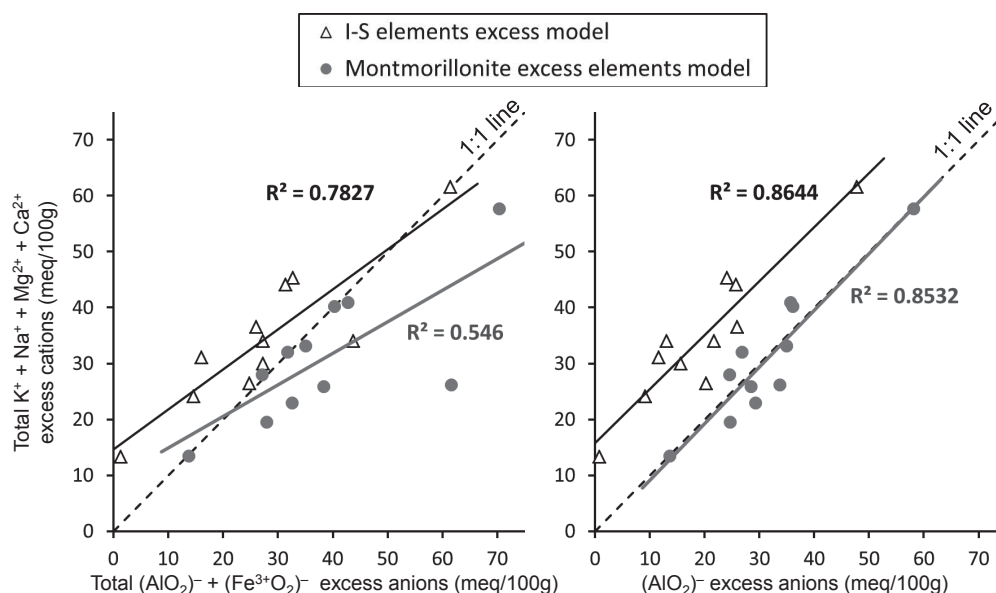


**FIGURE 8.** Total excess cations plotted against total excess anions for the opal-rich samples from the Monterey Formation, using I-S mineral model (Table 1b) and montmorillonite model (Table 1c) for excess element concentrations calculation. The black and gray trend lines correspond to the respective model data points; the  $R^2$  is given from the Major Axis (Model II) regression.

silicates within diatom particles. Most likely, such embedded smectite occurs mostly as monolayers, which is evidenced in the Monterey Formation opal-rich samples by the presence of the XRD  $hk0$  reflections that are proportionally much stronger than the corresponding  $00l$  reflections.

The presence of fine smectite crystallites (or even monolayers) associated with opal, in a combination with abundant Al substitutions in a silicate structure, suggests a specific pathway of smectite authigenesis in opals. The 1:1 charge ratio of total excess cations and Al implies the initial incorporation of tetrahedral Al into the silica network at an opal surface, rather than direct nucleation of smectite precursor at a solid-water interface that would have to lead to a significantly lower cation/Al ratio and the presence of octahedral Al. Although a formation of  $Al^{IV}$ -rich, highly anionic aluminosilicate gel at opal surface seems a feasible mechanism (Robertson and Twedily 1953; Michalopoulos et al. 2000; Houston et al. 2008), tetrahedral Al can also be incorporated directly into a diatom surface structure (Stoffyn 1979; Gehlen et al. 2002; Flörke et al. 2012). A mix of  $Al^{IV}$  and  $Al^{VI}$  found in natural diatoms (Gehlen et al. 2002) also supports the idea that above a certain concentration of heterogeneous cations incorporated in opal structure smectite layers can form. The authigenesis of smectite particles from such a heterogeneous cation composition in the opal structure can be facilitated by the opal dissolution-precipitation during the opal-A  $\rightarrow$  opal-CT transformation (Compton 1991; Williams and Crerar 1985).

### Water release from biogenic opals

Using the same approach as for the opal-normalized excess CEC calculation (Tables 1b and 1c),  $H_2O_{200}$  measured for the opal-rich samples (Table 1a) can be reduced by the theoretical water adsorbed on associated clay, using either the I-S model ( $H_2O_{200} = 7$  wt%) or the montmorillonite model ( $H_2O_{200} = 14$  wt%), assuming mixed Na and Ca cations in the interlayer (Środoń and McCarty 2008). The “excess  $H_2O_{200}$ ” values were then normalized to the opal content. These calculated  $H_2O_{200}$  values for pure opal from the Monterey Formation samples range from 2 to 4 wt% (Tables 1b and 1c), which is close to the  $H_2O_{200}$  values measured for the opal standards (3.5–5.3 wt%; Table 2).

Plotting the computed excess (opal)  $H_2O_{200}$  vs. excess (opal) CEC (Tables 1b and 1c) reveals a weak positive correlation for the opal-rich Monterey samples, regardless the detailed clay type assumed for the illite+smectite phase (Fig. 9). Moreover, both the modeled opal-A and opal-CT,  $CEC_{opal}$  and  $H_2O_{200,opal}$  values (Fig. 6), reduced by  $\sim 3\%$  contribution of virtual smectite, occur close to the trend line derived from the opal-rich Monterey samples. Although the actual opal  $H_2O_{200}/CEC$  ratio determined for these samples varies significantly from 0.3 to 1.0, a linear equation with an intercept of  $\sim 1.75$  wt% of  $H_2O_{200}$  for zero-CEC describes the opal  $H_2O_{200}$  and opal-CEC relationship with an average factor of 0.17 (SD = 0.066; Fig. 9). The very same  $H_2O_{200}/CEC$  ratio has been measured for pure smectite (Środoń and McCarty 2008; Kaufhold et al. 2010). Although these two values may be coincidental, they can as well suggest that a portion of the water removable from opal-A and -CT at 200 °C is controlled by the hydration of exchangeable cations like in expandable clays, and that content of such water varies among samples from the same formation. Alternatively, the linear correlation between CEC and

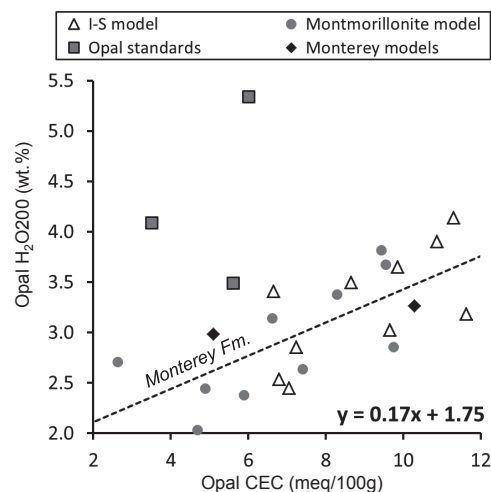


**FIGURE 9.** Excess (opal) CEC and excess (opal)  $H_2O_{200}$  values measured for opal standards (Table 2) and calculated for opal contribution after subtracting the illite+smectite contribution using I-S (Table 1b) and montmorillonite (Table 1c) models for the set of 12 opal-rich samples from the Monterey Formation. The results of  $CEC_{opal}$  and  $H_2O_{200,opal}$  modeling using the full sets of the Monterey Formation samples (opal-A zone and opal-CT zone = “Monterey models”), reduced for the contribution the virtual of 3% smectite, are also included. The linear correlation equation is given based on the Major Axis (Model II) regression for Monterey samples with both types of excess elements corrections (Tables 1b and 1c),  $n = 22$ ,  $r^2 = 0.500$ .

$H_2O_{200}$  can be provided by anhydrous, amorphous, Al-rich, gel-like aluminosilicate phase formed at opal surfaces (Robertson and Twedily 1953; Michalopoulos et al. 2000; Houston et al. 2008). In contrast, the other portion of adsorbed water in opal, described by the intercept, is cation-independent and it is relatively constant for the entire sample set. This fraction of water likely represents  $H_2O$  bound directly to Si-OH surface groups (Loucaides et al. 2010; Boboň et al. 2011). Two opal standards strongly deviate from the general trend of the  $H_2O_{200}$  vs. CEC in the Monterey Formation samples (Fig. 9). Such variability is not uncommon because opal surface properties can vary significantly (Van Cappellen 1996; Rodrigues et al. 1999; Boboň et al. 2011).

Because residual  $H_2O$  molecules are still noticeable in opal after drying in a vacuum at 200 °C (Boboň et al. 2011), the observed transition on the TG curve between the low-temperature and the high-temperature mass loss at  $\sim 300$  °C (Fig. 5) can be assigned to the complete removal of water molecules and the beginning of breaking O-H bonds in silanol groups. Further continuous mass loss, besides organic matter decomposition, is thus interpreted as subsequent dehydroxylation of silanol groups, forming  $H_2O$  molecules, starting from the opal surface and proceeding deeper into the opal structure. Water and OH groups may also be released from fluids contained in closed porosity (Khraisheh et al. 2005; Boboň et al. 2011).

As found in this study and by other authors,  $H_2O$  and OH contents vary significantly in opal-A and opal-CT structures (Jones and Renaut 2004; Boboň et al. 2011). The structural transition of opal-CT to opal-C and to chalcedony results, however, in an immediate loss of total water content (Graetsch et al. 1985) and

CEC (Table 2). The diagenetic reaction of opal-CT to opal-C must release enormous quantities of water, thus strongly change the local geochemical environment. Comparing the quantities of total water ( $\text{H}_2\text{O} + \text{OH}$ ) potentially releasable from opal (median content 48% with 6–12% water) and illite+smectite mineral group (median content 12% with 11–13% water), it appears that the total liquid locked up by opal in the Monterey Formation rocks can be much greater than the total  $\text{H}_2\text{O} + \text{OH}$  in clay minerals. When released by frictional heating during earthquakes, this expelled water can strongly affect the energetics and propagation of earthquakes (Hirono and Tanikawa 2011), which is especially significant in the neighboring San Andreas Fault system in central California.

### IMPLICATIONS

Different fractions of water in the opal structure and opal surface properties affect wireline log measurements and require a revision of the conventional approach to porosity determination. Not only the molecular weight divided by unit-cell volume (in ordered structures) or atomic weights and packing factor (in amorphous phases) are the controlling factors for mineral density, but also the quantity of OH groups and their surface distribution strongly affects the mineral density of opal-A and -CT (Chaika and Williams 2001; Boboň et al. 2011). The opal water would greatly mislead the wireline log-based neutron-porosity determination and may provide significant mismatch between the density, nuclear magnetic resonance (NMR), and resistivity logs when conventionally interpreted (Pearson and Derbyshire 1974; Clavier et al. 1984; LeCompte et al. 2008). The same tendency may occur when trying to calculate the CBW-equivalent for opals; the dual-water theory models will not be valid for opal-A and -CT in the same way as it works for clay minerals (Clavier et al. 1984; Fertl and Chilingar 1988; Matteson et al. 2000). Due to a multi-step mass loss during opals heating, there is no clear boundary between different fractions of  $\text{H}_2\text{O}$  and OH, therefore the notion of “dry mineral” in the case of opal-A and -CT may not have any practical meaning in oil exploration.

The relationship in Figure 9, gives hope for linking the conventional dual-water theory model to the opal-bound water. A portion of the opal-bound water can be CEC-dependent in a similar way as on the surfaces of clay minerals (Clavier et al. 1984; Kaufhold et al. 2010) while the intercept of the linear function of adsorbed water vs. CEC is probably a formation-specific constant that can be determined by careful mineralogical studies and quantitative analysis. The combined system of a constant  $\text{H}_2\text{O}$  in opal + variable  $\text{H}_2\text{O}$ , related to CEC as in smectite can potentially be applied for mineral modeling programs in wireline log formation evaluation (Fertl and Chilingar 1988; Brown and Ransom 1996; Zorski et al. 2011). Because two other opal standards do not follow the trend line formed by the Monterey samples, it is clear that separate studies are required for different basins.

As opposed to smectite, opal CEC may depend on the size of cation used for the CEC measurement in a similar manner as in zeolites (Robertson and Twedily 1953; Derkowski et al. 2006). Opal surface charge is pH-dependent with zero point charge at pH 5–6. At pH 10 opal surface charge density can increase to 0.5–0.6  $\text{C/m}^2$ , which is several times greater than smectite, while below pH 5 silica surface can develop anion exchange capacity (Rodrigues

et al. 2001; Ma et al. 2012). Such variability of opal surface properties with pH, within the pH range common for pore water chemistry, affects the reservoir stimulation process (Montgomery and Morea 2001). The adsorption of dyes as a function of pH was found, however, far less variable than the surface charge density (Khraisheh et al. 2005), so the opal surface adsorption properties under formation conditions may depend also on a type of adsorbate reagent used in a reservoir stimulation flow (cf. Robertson and Twedily 1953). Therefore, the CEC value measured for opal at a given pH in the laboratory can serve as reference but the actual formation CEC likely varies with the pH and chemical composition of pore water. Moreover, silanol pH-dependent surface properties may produce an alteration in opal surface wettability, from water-wet to oil wet, decreasing the efficiency of oil recovery (Turov and Leboda 1999; Strand et al. 2007).

### ACKNOWLEDGMENTS

Dale Julander and the Chevron Corporation San Joaquin Valley Business Unit team are greatly acknowledged for providing the samples, financial support, and permission to publish the results. We thank Bruce McCollum, Kimberli Correll, and Prince Ezebuio from Chevron ETC laboratories in Houston for essential laboratory work. Marta Labocha kindly helped with the statistics. We are grateful to Marek Szczerba for his criticism. Helpful comments and suggestions from the reviewer Panagiotis Michalopoulos and Warren Huff greatly improved the paper.

### REFERENCES CITED

- Badaud, D., and Risacher, F. (1983) Authigenic smectite on diatom frustules in Bolivian saline lakes. *Geochimica et Cosmochimica Acta*, 47, 363–375.
- Bardon, C., Bieber, M.T., Cuiec, L., Jacquin, C., Courbot, A., Deneuville, G., Simon, J.M., Voirin, J.M., Espy, M., Nectoux, A., and Pellerin, A. (1993) Recommandations pour la détermination expérimentale de la capacité d'échange de cations des milieux argileux. *Revue de l'Institut Français du Pétrole*, 38, 621–626.
- Beck, L., Gehlen, M., Flank, A.-M., Van Bennekom, A.J., and Van Beusekom, J.E.E. (2002) The relationship between Al and Si in biogenic silica as determined by PIXE and XAS. *Nuclear Instruments and Methods in Physics Research B*, 189, 180–184.
- Boboň, M., Christy, A.A., Klivanec, D., and Illášová, L. (2011) State of water molecules and silanol groups in opal minerals: a near infrared spectroscopic study of opals from Slovakia. *Physics and Chemistry of Minerals*, 38, 809–818.
- Brown, K.M., and Ransom, B. (1996) Porosity corrections for smectite-rich sediments: Impact on studies of compaction, fluid generation, and tectonic history. *Geology*, 24, 843–846.
- Chaika, C., and Williams, L.A. (2001) Density and mineralogy variations as a function of porosity in Miocene Monterey Formation oil and gas reservoirs in California. *AAPG Bulletin*, 85, 149–167.
- Clavier, C., Coates, G., and Dumanoir, J. (1984) Theoretical and experimental bases for the dual-water model for interpretation of shaly sands. *Society of Petroleum Engineers Journal*, 24, 153–168.
- Compton, J.S. (1991) Origin and diagenesis of clay minerals in the Monterey Formation, Santa Maria Basin area, California. *Clays and Clay Minerals*, 39, 449–466.
- Cortese, G., Gersonde, R., Hillenbrand, C.-D., and Kuhn, G. (2004) Opal sedimentation shifts in the World Ocean over the last 15 Myr. *Earth and Planetary Science Letters*, 224, 509–527.
- Derkowski, A., and Bristow, T.F. (2012) On the problems of total specific surface area and cation exchange capacity measurements in organic-rich sedimentary rocks. *Clays and Clay Minerals*, 60, 348–362.
- Derkowski, A., Franus, W., Beran, E., and Czimerová, A. (2006) Properties and potential applications of zeolitic materials produced from fly ash using simple method of synthesis. *Powder Technology*, 166, 47–54.
- Drits, V.A., and Tchoubar, C. (1990) X-ray Diffraction by Disordered Lamellar Structures, 371 p. Springer-Verlag, Berlin.
- Dohrmann, R. (2006) Cation exchange capacity methodology II: A modified silver-thiourea method. *Applied Clay Science*, 3, 38–46.
- Elzea, J.M., and Rice, S.B. (1996) TEM and X-ray diffraction evidence for cristobalite and tridymite stacking sequences in opal. *Clays and Clay Minerals*, 44, 492–500.
- Fertl, W.H., and Chilingar, G.V. (1988) Determination of volume, type, and distribution modes of clay minerals from well logging data. *Society of Petroleum Engineers Journal*, SPE-17145-MS, 13–28.
- Flörke, O.W., and 15 co-authors (2012) Silica. In *Ullmann's Encyclopedia of Industrial Chemistry*, 7<sup>th</sup> ed., p. 421–507. Wiley-VCH, Weinheim.



- Gaillou, E., Delaunay, A., Rondeau, B., Bouhnik-le-Coz, M., Fritsch, E., Cornen, G., and Monnier, Ch. (2008) The geochemistry of gem opals as evidence of their origin. *Ore Geology Reviews*, 34, 113–126.
- Gehlen, M., Beck, L., Calas, G., Flank, A.-M., Van Bennekom, A.J., and Van Beusekom, J.E.E. (2002) Unraveling the atomic structure of biogenic silica: Evidence of the structural association of Al and Si in diatom frustules. *Geochimica et Cosmochimica Acta*, 66, 1601–1609.
- Graetsch, H., Flörke, O.W., and Miehe, G. (1985) The nature of water in chalcedony and opal-C from Brazilian agate geodes. *Physics and Chemistry of Minerals*, 12, 300–306.
- Guthrie, G.D. Jr., Bish, D.L., and Reynolds, R.C. Jr. (1995) Modeling the X-ray diffraction pattern of opal-CT. *American Mineralogist*, 80, 869–872.
- Hirono, T., and Tanikawa, W. (2011) Implications of the thermal properties and kinetic parameters of dehydroxylation of mica minerals for fault weakening, frictional heating, and earthquake energetics. *Earth and Planetary Science Letters*, 307, 161–172.
- Houston, J.R., Herberg, J.L., Maxwell, R.S., and Carroll, S.A. (2008) Association of dissolved aluminum with silica: Connecting molecular structure to surface reactivity using NMR. *Geochimica et Cosmochimica Acta*, 72, 3326–3337.
- Huang, W.L., Longo, J.M., and Pevear, D.R. (1993) An experimentally derived kinetic model for smectite-to-illite conversion and its use as a geothermometer. *Clays and Clay Minerals*, 41, 162–177.
- Jackson, M.L. (1969) *Soil Chemical Analysis—Advanced course*, 2<sup>nd</sup> ed. Self-published, Madison, Wisconsin, U.S.A.
- Jones, B., and Renaut, R.W. (2004) Water content of opal-A: Implications for the origin of laminae in geyserite and sinter. *Journal of Sedimentary Research*, 74, 117–128.
- Kaufhold, S. (2006) Comparison of methods for the determination of the layer charge density (LCD) of montmorillonites. *Applied Clay Science*, 34, 14–21.
- Kaufhold, S., Dohrmann, R., and Klinkenberg, M. (2010) Water-uptake capacity of bentonites. *Clays and Clay Minerals*, 58, 37–43.
- Keller, M.A., and Isaacs, C.M. (1985) An evaluation of temperature scales for silica diagenesis in diatomaceous sequences including a new approach based on the Miocene Monterey Formation, California. *Geo-Marine Letters*, 5, 31–35.
- Khraisheh, M.A.M., Al-Ghouti, M.A., Allen, S.J., and Ahmad, M.N. (2005) Effect of OH and silanol groups in the removal of dyes from aqueous solution using diatomite. *Water Research*, 39, 922–932.
- Koning, E., Gehlen, M., Flank, A.-M., Calas, G., and Epping, E. (2007) Rapid post-mortem incorporation of aluminum in diatom frustules: Evidence from chemical and structural analyses. *Marine Chemistry*, 106, 208–222.
- Loucaides, S., Behrend, T., and Van Cappellen, P. (2010) Reactivity of biogenic silica: Surface versus bulk charge density. *Geochimica et Cosmochimica Acta*, 74, 517–530.
- LeCompte, B., Mendez, F., Jacobi, D., and Longo, J. (2008) Defining clay type using NMR and geochemical logging measurements, p. 1–9. Society of Petrophysicists and Well Log Analysts 49<sup>th</sup> Annual Logging Symposium, U.K.
- Ma, W., Song, X., Pan, Y., Cheng, Z., Xin, G., Wang, B., and Wang, X. (2012) Adsorption behavior of crystal violet onto opal-And reuse feasibility of opal-dye sludge for binding heavy metals from aqueous solutions. *Chemical Engineering Journal*, 193–194, 381–390.
- Matheny, R.K., and Knauth, L.P. (1993) New isotopic temperature estimates for early silica diagenesis in bedded cherts. *Geology*, 21, 519–522.
- Matteson, A., Tomanic, J.P., Herron, M.M., Allen, D.F., and Kenyon, W.E. (2000) NMR relaxation of clay/brine mixtures. *SPE Reservoir Evaluation & Engineering*, 3, 408–413.
- McCarty, D.K., Sakharov, B.A., and Drits, V.A. (2008) Early clay diagenesis in Gulf Coast sediments: New insights from XRD profile modeling. *Clays and Clay Minerals*, 56, 359–379.
- (2009) New insights into smectite illitization: A zoned K-bentonite revisited. *American Mineralogist*, 94, 1653–1671.
- Mendioroz, S., Belzunce, M.J., and Pajares, J.A. (1989) Thermogravimetric study of diatomites. *Journal of Thermal Analysis*, 35, 2097–2104.
- Michalopoulos, P., Aller, R.C., and Reeder, R.J. (2000) Conversion of diatoms to clays during early diagenesis in tropical, continental shelf muds. *Geology*, 28, 1095–1098.
- Montgomery, S.L., and Morea, M.F. (2001) Antelope shale (Monterey Formation), Buena Vista Hills field: Advanced reservoir characterization to evaluate CO<sub>2</sub> injection for enhanced oil recovery. *AAPG Bulletin*, 85, 561–585.
- Omotoso, O., McCarty, D.K., Hillier, S., and Kleeberg, R. (2006) Some successful approaches to quantitative mineral analysis as revealed by the 3rd Reynolds Cup contest. *Clays and Clay Minerals*, 54, 748–760.
- Orsini, L., and Remy, J.C. (1976) Utilisation du chlorure de cobalt hexammine pour la détermination simultanée de la capacité d'échange et des bases échangeables des sols. *Science du sol*, 4, 269–275.
- Pearson, R.T., and Derbyshire, W. (1974) NMR studies of water adsorbed on a number of silica surfaces. *Journal of Colloid and Interface Science*, 46, 232–248.
- Robertson, R.H.S., and Tweddy, A.E. (1953) The biogeochemistry of Skye diatomite. *Clay Minerals Bulletin*, 2, 7–16.
- Rodrigues, F.A., Monteiro, P.J.M., and Sposito, G. (1999) The alkali-silica reaction. The surface charge density of silica and its effect on expansive pressure. *Cement and Concrete Research*, 29, 527–530.
- (2001) The alkali-silica reaction. The effect of monovalent and bivalent cations on the surface charge of opal. *Cement and Concrete Research*, 31, 1549–1552.
- Rondeau, B., Cenki-Tok, B., Fritsch, E., Mazzerio, F., Gauthier, J.P., Bodeur, Y., Bekele, E., Gaillou, E., and Ayalew, D. (2012) Geochemical and petrological characterization of gem opals from WegelTena, Wollo, Ethiopia: Opal formation in an Oligocene soil. *Geochemistry: Exploration, Environment, Analysis*, 12, 93–104.
- Sakharov, B.A., Lindgreen, H., Salyn, A.I., and Drits, V.A. (1999) Determination of illite-smectite structures using multispecimen X-ray diffraction profile fitting. *Clays and Clay Minerals*, 47, 555–566.
- Shukla, S.K., and Mohan, R. (2012) The contribution of diatoms to worldwide crude oil deposits. In R. Gordon and J. Seckbach, Eds., *The Science of Algal Fuels*, p. 355–382. Springer, Dordrecht.
- Stoffyn, M. (1979) Biological control of dissolved aluminium in seawater: Experimental evidence. *Science*, 203, 651–653.
- Strand, S., Hjuler, M.L., Torsvik, R., Pedersen, J.I., Madland, M.V., and Austad, T. (2007) Wettability of chalk: Impact of silica, clay content and mechanical properties. *Petroleum Geoscience*, 13, 69–80.
- Środoń, J. (2009) Quantification of illite and smectite and their layer charges in sandstones and shales from shallow burial depth. *Clay Minerals*, 44, 421–434.
- Środoń, J., and McCarty, D.K. (2008) Surface area and layer charge of smectite from CEC and EGME/H<sub>2</sub>O-retention measurements. *Clays and Clay Minerals*, 56, 155–174.
- Środoń, J., Drits, V.A., McCarty, D.K., Hsieh, J.C.C., and Eberl, D.D. (2001) Quantitative XRD analysis of clay-rich rocks from random preparations. *Clays and Clay Minerals*, 49, 514–528.
- Środoń, J., Zeelmaekers, E., and Derkowski, A. (2009) The charge of component layers of illite-smectite in bentonites and the nature of end-member illite. *Clays and Clay Minerals*, 57, 650–672.
- Turov, V.V., and Leboda, R. (1999) Application of <sup>1</sup>H NMR spectroscopy method for determination of characteristics of thin layers of water adsorbed on the surface of dispersed and porous adsorbents. *Advances in Colloid and Interface Science*, 79, 173–211.
- Van Bennekom, A.J., and van der Gaast, S.J. (1976) Possible clay structures in frustules of living diatoms. *Geochimica et Cosmochimica Acta*, 40, 1149–1152.
- Van Cappellen, P. (1996) Reactive surface area control of the dissolution kinetics of biogenic silica in deep-sea sediments. *Chemical Geology*, 132, 125–130.
- Webb, J.A., and Finlayson, B.L. (1987) Incorporation of Al, Mg, and water in opal-A: Evidence from speleothem. *American Mineralogist*, 72, 1204–1210.
- Williams, L.A., and Crerar, D.A. (1985) Silica diagenesis: II, General mechanisms. *Journal of Sedimentary Petrology*, 55, 312–321.
- Zorski, T., Ossowski, A., Środoń, J., and Kawiak, T. (2011) Evaluation of mineral composition and petrophysical parameters from well logging data: The Carpathian Foredeep case study. *Clay Minerals*, 46, 25–45.

MANUSCRIPT RECEIVED APRIL 13, 2014

MANUSCRIPT ACCEPTED OCTOBER 29, 2014

MANUSCRIPT HANDLED BY WARREN HUFF